Mechanism for the uniaxial strain dependence of the critical current in practical REBCO tapes

2016 Supercond. Sci. Technol. 29 065019

(http://iopscience.iop.org/0953-2048/29/6/065019)

IOP Publishing Superconductor Science and Technology
Supercond. Sci. Technol. **29** (2016) 065019 (17pp) doi:10.1088/0953-2048/29/6/065019

Mechanism for the uniaxial strain dependence of the critical current in practical REBCO tapes

Kozo Osamura[1], Shutaro Machiya[2] and Damian P Hampshire[3]

[1] Research Institute for Applied Sciences, Kyoto 606-8202, Japan
[2] Department of Engineering, Daido University, Nagoya 457-8530, Japan
[3] Department of Physics, University of Durham, Durham DH1 3LE, UK

E-mail: kozo_osamura@rias.or.jp

Received 31 January 2016, revised 14 April 2016
Accepted for publication 15 April 2016
Published 6 May 2016

Abstract

In order to elucidate the effect of uniaxial strain on the critical current of practical REBCO tapes ($REBa_2Cu_3O_{7-d}$, RE = Y and Gd) fabricated by Superpower and SuNAM, two types of critical current measurements were carried out. In the first, the tape sample was attached directly to a universal testing machine and pulled under a tensile load. In the second, the tape was soldered to a Cu–Be springboard and then attached to the testing machine and then pushed or pulled in order to apply both tensile and compressive strains to the tape sample. An inverse parabolic behaviour was observed for the uniaxial strain dependence of the critical current of both tapes. Using synchrotron radiation, the local strain exerted on the REBCO layer was measured at room temperature under the conditions used for the two techniques for making I_c measurements. On the basis of these room temperature data, the local strain exerted on the REBCO layer at 77 K was numerically evaluated. A one-dimensional chain model for current flow in the REBCO material with fractional lengths of A-domains and B-domains oriented along the uniaxial strain direction is proposed. The model can explain the parabolic strain behaviour of the critical current and shows that the strain at which the peak in I_c occurs, is not only determined by pre-compression or pre-tension on the superconductor at the operating temperature, but also by the ratio of the fractional amounts of the two domains.

Keywords: critical current, uniaxial strain dependence, REBCO coated conductor, synchrotron radiation, thermal strain, chain model, twin structure

(Some figures may appear in colour only in the online journal)

1. Introduction

A superconducting wire or tape can be regarded as a 'practical one' when it can be procured in sufficiently continuous lengths under ordinary commercial transactions to build devices as described in the document [1]. Five kinds of composite superconductors consisting of the alloy Nb–Ti, Nb_3Sn, MgB_2 intermetallic compound, BSCCO ($Bi_2Sr_2Ca_nCu_{n+1}O_{6+2n}$; $n = 1$ and 2) and REBCO ($REBa_2Cu_3O_{6+x}$; RE = Y, Gd and Sm) oxides are commercialized at present. Their shapes are either round wires or tapes.

Practical SC wires and tapes are composites that meet the desired engineering characteristics following expert selection of materials and the ingenious design of the architecture. Because of the differences in the coefficient of thermal expansion (CTE) and the modulus of elasticity among the constituent components, the macroscopic mechanical properties of composites are complicated and make it difficult to determine simply the local strain exerted on the superconducting component that influences its electromagnetic properties under operation [2]. Some analysis of the local stresses and strains that are generated throughout the interior

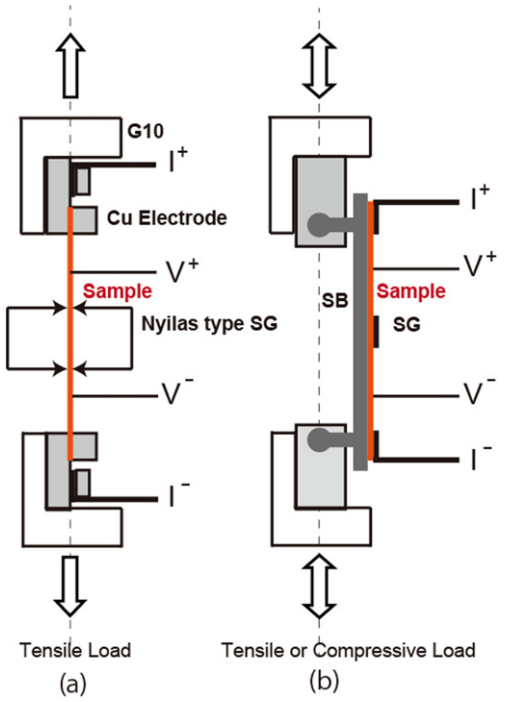

Figure 1. Two techniques for evaluating the uniaxial strain dependence of I_c, where G10 is an insulator, SG is a strain gauge, and SB is the springboard.

of BSCCO [3], REBCO [4] and Nb_3Sn [5, 6] composites have been reported in the literature.

In many practical SC wires, the existence of a maximum in critical current (I_c) versus uniaxial strain has been widely reported. The peak in I_c found in practical Nb_3Sn wires has been well established experimentally. The usual explanation includes a co-incidence between the highest superconducting properties and zero deviatoric strain in this material [7]. Because of the prevalence of the peak in I_c versus strain in many SC wires, most papers report the critical current versus strain data in terms of intrinsic strain (A_i) which is defined by $A_i = A_a - A_p$ where A_a is the applied strain and A_p is the peak strain at which I_c reaches its maximum value. Recently a benchmarking experiment was conducted to compare strain measurement facilities at two research institutes [8] that use a Cu–Be Walters' spring strain device and a Ti-6Al-4V Pacman bending beam apparatus. The critical current of the same bronze-route Nb_3Sn wire was measured as a function of axial strain and magnetic field in liquid helium at both institutes and showed that although the peak in I_c occurs at different applied strains, A_p is nearly the same as the strain at which the so-called force free strain (A_{ff}) appears [9]. These results demonstrate that it is important to make clear the relationship between the peak strain and the local strain exerted on the SC component itself. For practical REBCO and BSCCO wires, a maximum in the critical current has also been observed in the strain dependence. In studies to date, A_p tended to be inconsistent with A_{ff} [10, 11]. It is the aim of this work to understand better the true nature of the critical current maximum and its dependence on strain by explicitly examining directly, the change of critical current as a function of local strain exerted on the SC component.

Table 1. Characteristic dimensions of the components of the REBCO tapes, where values denoted by the star * were measured in-house and the others were taken from the manufacturer specifications.

Sample name	Superpower	SuNAM
Tape thickness (mm)	0.095*	0.19*
Tape width (mm)	4.04	4.02
Hastelloy substrate (μm)	50	60
Cu Lamination (μm)	40	120
REBCO thickness (μm)	1	1.0–1.5
Rare earth element	$Y_{0.5}Gd_{0.5}$	Gd

In order to compare the strain dependence of the critical current over a wide range of uniaxial strain, two techniques were employed in the present study. In the first, as shown in figure 1(a), the sample holder is freestanding, attached to the universal testing machine and is pulled using a tensile load. The tape sample is gripped by two copper electrodes, which are insulated from the tensile machine by means of G10 insulators. Under an applied tensile load, the *E–I* characteristics are measured and the critical current determined, while the strain is monitored by means of the Nyilas type strain gauge. Unfortunately, it is not possible to apply a compressive load to the tape sample using this technique because the sample buckles.

In order to measure the critical current in both compressive and tensile strains, we employed a springboard (SB) in the second type of experiment as shown in figure 1(b) [12]. A tape-sample is soldered onto the SB and a strain gauge is glued onto the sample surface. Then applying either tensile or compressive load, it becomes possible to measure the uniaxial strain dependence of the critical current for positive and negative strains. When comparing the strain dependences obtained by means of the different types of measurements shown in figure 1, it is essential to consider the thermal strain exerted on the superconducting layer. Hence in the present study, we have also evaluated quantitatively the thermally induced strain on the superconducting layer using synchrotron measurements and used it to find the local strain so we can discuss its influence on the uniaxial strain dependence of critical current.

2. Experimental procedure

Two kinds of commercialized REBCO superconducting tapes were used as test samples. They have been acquired from Superpower and SuNAM and their general specifications are listed in table 1 and on the manufacturer's web-pages [13, 14]. Broadly the tapes consist of a thin superconducting layer, grown on the substrate via a buffer layer, which is laminated with a copper layer.

In the present study, the thermal history experienced by the sample was carefully controlled. As shown in figure 2(a), the tape was cooled after the manufacturing process is

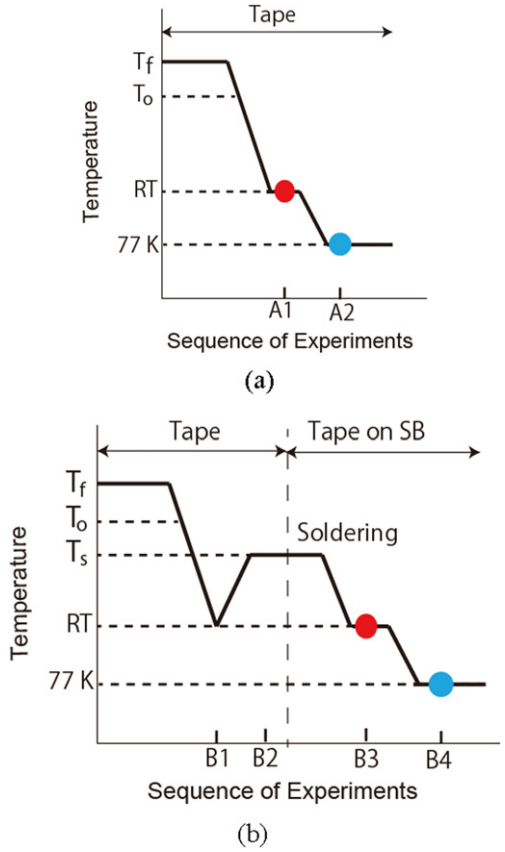

Figure 2. Thermal history and sample preparation in the present experiments. (a) The free standing tape and (b) the tape mounted on a spring board.

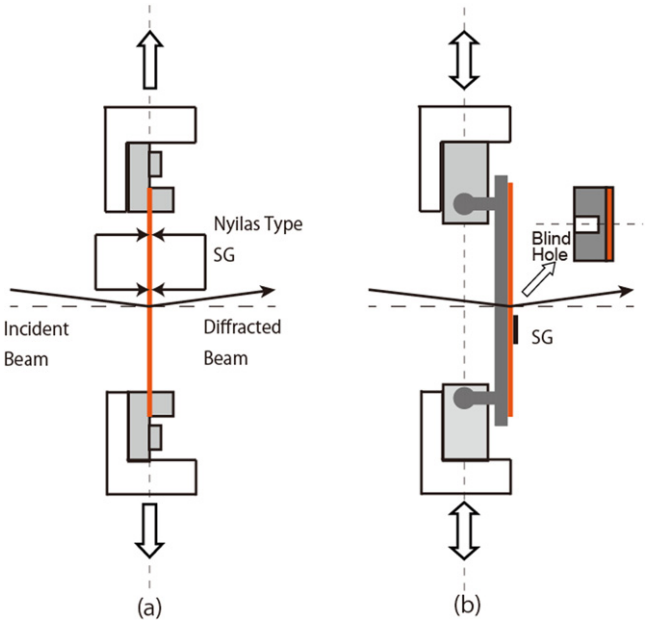

Figure 3. Sample holders for diffraction experiments.

finished at T_f. Due to the difference in CTE among the constituent elements, thermal strains start to be induced at T_o during cooling. In general, a determination of T_o is difficult, but is evaluated in this paper using numerical analysis. When a tape is mounted on a SB, the corresponding thermal history is more complicated as depicted in figure 2(b). The tape is heated to the soldering temperature and then mounted on the SB. Then it is cooled down to 77 K for I_c measurements. We note that samples were not re-used—different lengths of tape were used for each of the measurements presented in this work. The local strain measurements were carried out at room temperature at steps A1 and B3 in figure 2. The I_c measurements were performed at 77 K at steps A2 and B4.

The diffraction experiments were carried out at room temperature at the BL45XU station of SPring-8. It used white x-rays with energies between 30 and 150 keV and a cooled Ge solid-state detector set to a diffraction angle of $2\theta = 8°$. As with the critical current measurements, a freestanding sample and a sample on a SB were measured. For the freestanding sample, as shown in figure 3(a), the Nyilas type SG was placed outside the diffraction point of the incident beam to prevent it from absorbing any of the incident beam. The sample on the SB was installed in a specially designed load frame, which was placed at the centre of the goniometer. The size of the Cu–Be SB was 78 mm long, 15 mm wide and 2.5 mm thickness. In order to reduce the absorption of the incident beam, a blind hole was incorporated into the spring board.

In both cases, the diffraction peaks were measured as a function of uniaxial strain. This involved measuring the change of the diffraction angles produced by the component materials as a function of tensile strain. The diffraction geometry ensured that the scattering vector was parallel to the tape axis. Several diffraction peaks belonging to {h00}, {0k0} and {hk0} crystal planes of the orthorhombic REBCO were observed. In the present study, the spacing of the {h00} and {0k0} planes was employed for local strain measurements because their diffraction intensity was strong enough to ensure sufficient statistical accuracy.

The critical current measurements were carried out in a liquid nitrogen filled open cryostat. The freestanding sample was held using a gripping jig which was electrically isolated from the universal testing machine Shimadzu AG-50kNIS (figure 1(a)). The voltage taps were soldered onto the tape, 25 mm apart, outside the Nyilas type gauge. The critical current was determined with a criterion of 1 μV cm^{-1}. For the measurements on the SB (figure 1(b)), the tape sample was soldered onto the SB using the eutectic solder (Sn-37% Pb), and a strain gauge, 4 mm long and 2.7 mm wide, was glued onto the tape surface. The voltage taps were soldered onto the tape, 25 mm apart, outside the strain gauge. The critical current measurement was carried out after attaching the SB to the universal testing machine. Compressive and tensile strains were applied to the tapes by pushing or pulling along the load axis and measuring the changes in strain produced using the strain gauge.

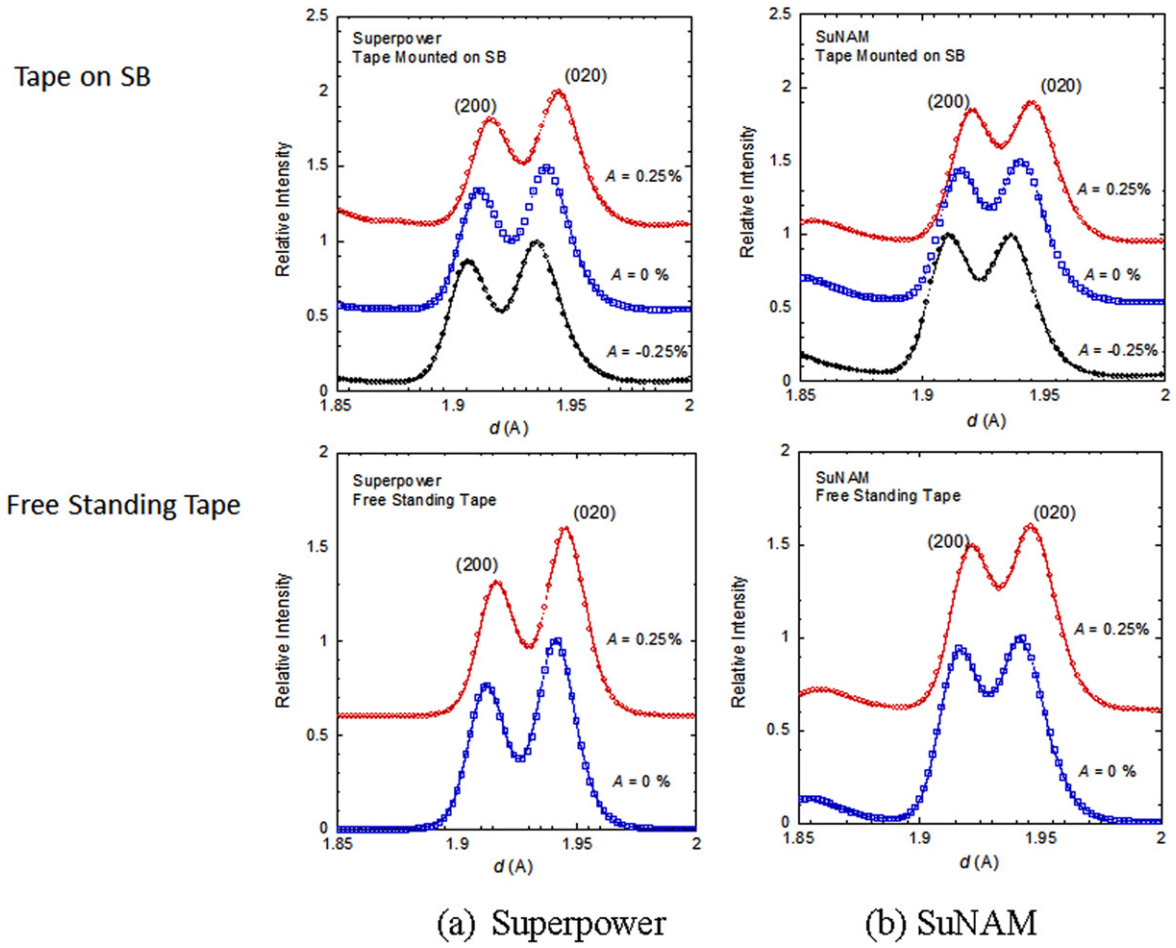

Figure 4. Diffraction profile of (200) and (020) crystal planes under the axial strains as a function of lattice spacing for two kinds of tapes at room temperature. (a) Superpower (b) SuNAM.

3. Experimental results

3.1. Definitions of terms used to characterize the local strain

Synchrotron measurements at room temperature were used to get direct information about the local strain exerted on the REBCO superconducting layer and investigate properly its effect on critical current. As shown in figure 4, two diffraction peaks were observed corresponding to the (200) and (020) crystal planes, where the scattering vector was kept to be parallel to the tape axis. As expected, their peak positions shift towards larger lattice spacing, when the axial strain was increased from −0.25% to +0.25%. The diffraction intensity of the (020) crystal planes are similar but generally larger than those of the (200) planes under all applied strain conditions. However, one has to be careful about detailed quantitative comparisons of diffraction intensities between the two peaks of the (200) and (020) planes. In the twinned structure, both planes are inclined to each other by 0.96° owing to the difference of their crystal lattice constant [4]. Therefore it is not possible to keep the scattering vector parallel to both inverse lattice vectors at the same time which undermines detailed quantitative analysis.

In order to know the strain-free state, fine REBCO powder was extracted from the same tape sample. Such isolated homogeneous powder with a size less than a few μm is expected to carry no residual strain. We denote the crystal plane spacing of the powder at arbitrary temperature, T, under strain-free conditions and zero applied strain (A_a) as $d^{p}_{REBCO}(T, 0)$. In this paper we use the crystal plane spacing of the powder at room temperature as the primary experimental reference point to define the strain-free plane spacing at 293 K, d^{p}_{REBCO} (293 K, 0). Hence, the thermal strain in the tape is given by the equation

$$A^{T}_{REBCO} = \frac{d_{REBCO}(T, 0) - d^{p}_{REBCO}(T, 0)}{d^{p}_{REBCO}(T, 0)} 100 \quad [\%]. \quad (1)$$

When an external strain is applied to the tape sample, the REBCO layer elongates or shrinks and the crystal plane spacing changes from $d_{REBCO}(T, 0)$ to $d_{REBCO}(T, A_a)$. We define the lattice strain in the practical manner as

$$A^{lat}_{REBCO}(A_a) = \frac{d_{REBCO}(T, A_a) - d_{REBCO}(T, 0)}{d_{REBCO}(T, 0)} 100 \quad [\%]. \quad (2)$$

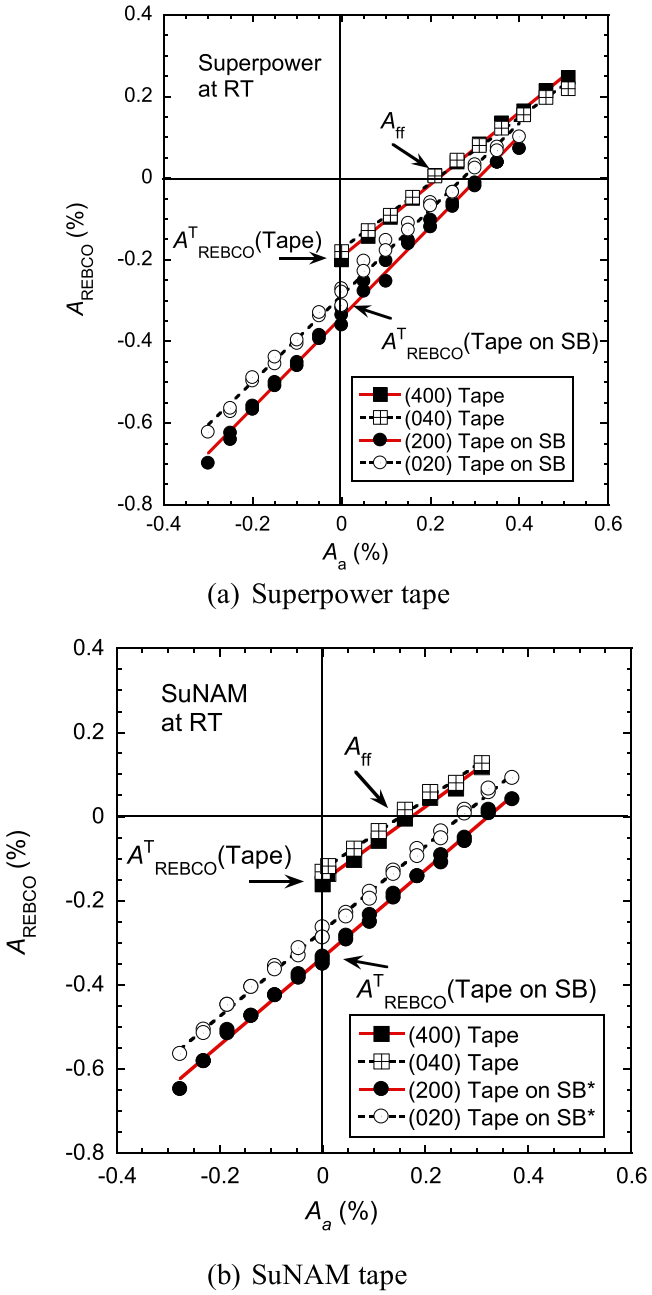

Figure 5. Change of local strain exerted on REBCO layer as a function of applied strain at room temperature for the freestanding tape and the tape mounted on the SB. (a) Superpower tape (b) SuNAM tape.

The local strain exerted on the REBCO layer is the sum of the thermal strain and lattice strain and is defined by the equation

$$A_{\mathrm{REBCO}}(A_{\mathrm{a}}) \equiv A^{\mathrm{T}}_{\mathrm{REBCO}} + A^{\mathrm{lat}}_{\mathrm{REBCO}}(A_{\mathrm{a}}). \tag{3}$$

The change of local strain exerted on REBCO layer is shown in figure 5 for both tapes. The applied strain dependence of A_{REBCO} is linear and given by:

$$A_{\mathrm{REBCO}}(A_{\mathrm{a}}) = A^{\mathrm{T}}_{\mathrm{REBCO}} + \frac{\mathrm{d}A^{\mathrm{lat}}_{\mathrm{REBCO}}}{\mathrm{d}A_{\mathrm{a}}} A_{\mathrm{a}}. \tag{4}$$

3.2. The local strain exerted on the REBCO superconducting layer at room temperature

When the tape sample is soldered to the SB and strain applied by pushing or pulling the legs of the SB, the strain is predominantly uniaxial. However there is also a non-negligible bending strain because of the finite thickness of tape. However, as discussed previously [11], the contribution from the bending strain component was not considered in the present study, because its influence is quite limited. Because the strain gauge is further from the neutral axis of the SB than the REBCO layer, caused by the thickness of the Cu lamination, the thickness of the glue for the strain gauge and the half-thickness of the strain gauge itself, the measured strain has been corrected by multiplying a factor k. The procedure to evaluate the factor k is explained in the appendix. The uniaxial strain dependence of the local strain on REBCO layer was observed for both the SuNAM and the Superpower tape. Figure 5 shows the experimental results after processing the correction. Both as-supplied tapes have the REBCO under compression at room temperature. Equation (4) was curve-fitted to the observed data shown in figure 5 and the slopes of proportionality and the intercept were evaluated and are listed in table 2. Furthermore, an important strain parameter is the force free strain (A_{ff}) at the operating temperature for I_{c} measurements [15]. The force free strain at 293 K is shown for the Superpower tape and the SuNAM tape in figure 5 (and below in figure 9 at 77 K following the calculations given in section 3.3).

Table 2 shows the slope of $A^{\mathrm{lat}}_{\mathrm{REBCO}}$ versus A_{a} is not unity, but shows systematic changes such that the slope for the tapes mounted on the SB are higher than that for the free standing tapes. Furthermore the slope for (020) planes is smaller than that for (200) ones. These results are attributed to the following reasons. When a uniaxial stress is applied to the polycrystalline sample, individual grains deform along the force axis by an amount proportional to elastic constant and specified to its own crystal orientation. This phenomenon is well known from discussions of the elastic properties obtained using other diffraction data on the REBCO coated conductors consider here in which micro-twins are distributed in the grains [16]. The smaller slope along [010] axis is attributed to the larger elastic constant in this direction as reported previously [4]. The origin of the larger slope for the tape mounted on the SB is unsolved problem at present.

3.3. Evaluation of thermal strain exerted on REBCO layer at 77 K

The present REBCO tapes are typical composite superconducting materials consisting of five components as listed

Table 2. Thermal strain, the slope and the force free strain at 293 K.

		SP			SuNAM		
	{h00}	A^{T}_{REBCO} (%)	$\frac{dA^{lat}_{REBCO}}{dA_a}$	A_{ff} (%)	A^{T}_{REBCO} (%)	$\frac{dA^{lat}_{REBCO}}{dA_a}$	A_{ff} (%)
Free-standing Tape	(400)	−0.21	0.88	0.21	−0.16	0.89	0.18
	(040)	−0.19	0.80	0.21	−0.14	0.83	0.16
Tape on SB	(200)	−0.34	1.17	0.29	−0.32	1.04	0.33
	(020)	−0.29	1.11	0.25	−0.28	1.01	0.27

Table 3. Volume fraction of components in both Superpower and SuNAM tapes.

		V_{fi} (%)	
i	Component	SP	SuNAM
1	REBCO	1.1	1.6
2	buffer	0.2	0.1
3	Hastelloy	52.6	65.1
4	Ag	4.0	0.6
5	Cu	42.1	32.5

in table 3. Due to the different CTE of the constituent components, a thermal strain is generated in each component when the sample is cooled down from high temperature. The principal procedure to evaluate the thermal strain has been discussed previously [3]. As shown in figure 5, and table 2, the thermal strain exerted on the REBCO layer at room temperature was directly measured in the present study. The local strain state is a function not just of temperature, but also history because Cu behaves in an elasto-plastic manner and yields mechanically due to the increase of local stress during the cooling and heating processes as is discussed and evaluated below.

(a) Process from T_0 to room temperature.

As shown in figure 2, the tape is cooled down from temperature T_f, after the heat treatment, to form the REBCO SC phase. We assume there is a specific temperature (T_0) [21], at which the thermal strain exerted on REBCO layer starts in practice and evaluate it. The thermal strain exerted on component i is defined as A_i^T, where from the definition of T_0, $A_i^{T_0} = 0$ at $T = T_0$ ($i = 1, 2, 3, 4$ and 5). During cooling, the whole tape shrinks. All components shrink by an amount roughly proportional to the average CTE (α_c). The thermal strain of component i is given as a function of the term (α_i–α_c) where α_i is the CTE of component i. In general, the CTE of any material is a nonlinear function of temperature. Data of CTE used for the present calculations were as follows; temperature dependent data for Cu [5], Hastelloy [17] and Cu–Be [18, 20] and constant values at room temperature for the oxides [19] and REBCO [18]. In the current calculations, the parameters were extrapolated over the necessary temperature range.

When cooling down to T, the thermal strain of component i is given by

$$A_i^T = \int_T^{T_o} (\alpha_i - \alpha_c) dT. \quad (5)$$

The corresponding thermal stress in component i is given by R_i^T. All the thermal stresses balance, consistent with the following constraint condition from the rule of mixtures

$$V_{f1}R_1^T + V_{f2}R_2^T + V_{f3}R_3^T + V_{f4}R_4^T + V_{f5}R_5^T = 0. \quad (6)$$

This condition assumes that the composite system shrinks as a whole during cooling so that anyone of constituent components does not shrink separately. In the experiments reported here this assumption holds, although we note that at the interface between REBCO film and buffer layers there is no perfect epitaxy so the mechanical rigidity of the interface is rather soft. Equation (5) includes only one unknown variable α_c. The thermal stress is introduced as a function of the thermal strain as given by equations (7) and (8). Equation (6) is the sum of those thermal stresses. Then α_c is determined by solving equation (6).

After calculating the temperature dependence of α_c, one can integrate equation (5) to find the thermal strain of each component. The relation between stress and strain in the pertinent strain region of the present study was calculated as follows. The three components: REBCO, oxides and Hastelloy, behave elastically

$$R_i^T = E_i A_i^T, \quad (7)$$

where E_i is the modulus of elasticity of component i. Ag and Cu have small elastic limits and so yield quite quickly and behave elasto—plastically. As discussed previously [21], their stress versus strain relation is given as

$$R_i^T = \frac{E_i b_i (A_i^T)^{1+1/ni}}{E_i A_i^T + b_i (A_i^T)^{1/ni}}, \quad (8)$$

where the b_i and n_i are fitting parameters and their values were reported in the previous papers [5, 21].

Using the procedure mentioned above, the strains exerted on the REBCO layer (A^T_{REBCO}) at 293 and 77 K, were numerically evaluated as a function of T_0 as shown in figure 6 for Superpower tape. The thermal strain on REBCO layer is compressive and increases with increasing T_0. In order to determine the temperature T_0 , the numerical results shown in figure 6 were compared with the observed thermal strain of

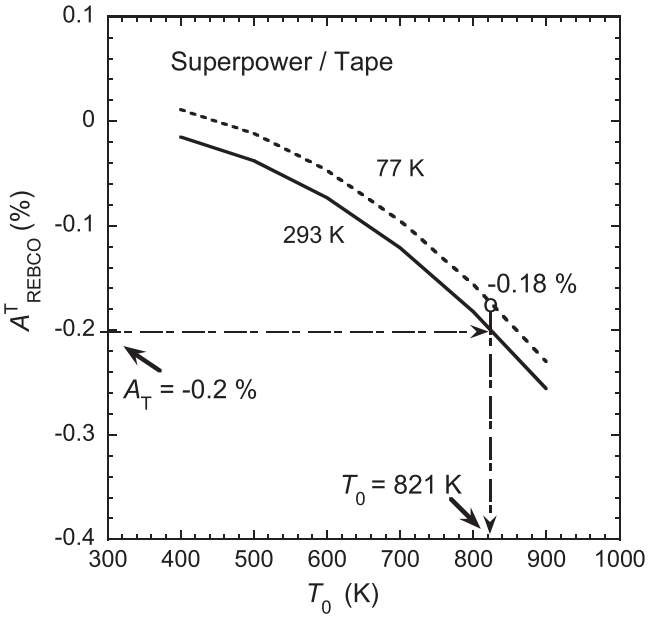

Figure 6. Thermal strain exerted on the REBCO layer at 293 and 77 K as a function of T_0 in the Superpower tape.

Table 4. Local strain on REBCO layer for the freestanding tape and the tape on the SB before and after soldering. The starred* values are angular averages taken from table 2.

		A^T_{REBCO} (%)	
Step	T (K)	SP	SuNAM
A1 and B1	293	−0.20*	−0.15*
A2	77	−0.18	−0.12
B2	460	−0.19	−0.15
B3	293	−0.31	−0.27
B4	77	−0.41	−0.38

Table 5. Volume fraction of components in both Superpower and SuNAM tapes mounted on the springboard.

		V_{fi} (%)	
i	Component	SP	SuNAM
1	REBCO	0.013	0.021
2	buffer	0.003	0.001
3	Hastelloy	0.658	0.857
4	Ag	0.050	0.008
5	Cu	0.526	0.428
6	Cu–Be	98.74	98.78

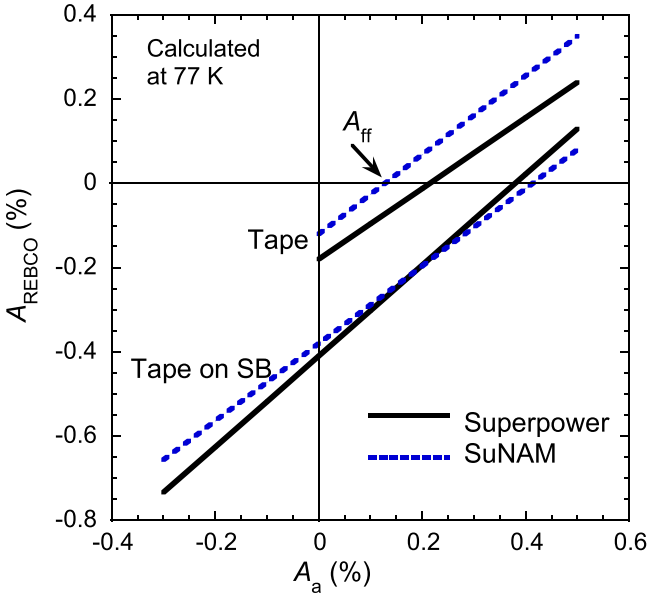

Figure 7. The calculated local strain exerted on the REBCO layer at 77 K as a function of applied strain for both the Superpower tape and the SuNAM tape when freestanding and when mounted on SB.

−0.20% at 293 K—the average value of the (400) and (040) data listed in table 2—and T_0 was found to be 821 K. The thermal strain on REBCO at 77 K is then given as $A^{77}_{REBCO} = -0.18\%$ from figure 6. Using the same procedure for the SuNAM tape, T_0 was estimated as 779 K by using an average value of thermal strain of −0.15% at 293 K (see table 2) and the thermal strain at 77 K was calculated to be $A^{77}_{REBCO} = -0.12\%$.

(b) Steps B1–B2: from room temperature to the soldering temperature.

Each tape was heated from room temperature to the soldering temperature (T_s) as shown in figure 2. The thermal strain on component i at T_s is given by the equation

$$A_i^{Ts} = \int_{RT}^{T_0} (\alpha_i - \alpha_c)\mathrm{d}T + \int_{Ts}^{RT} (\alpha_i - \alpha_c)\mathrm{d}T. \qquad (9)$$

The constraint condition equation (6) was solved by using equation (9). In the present case, the soldering temperature was $T_s = 460$ K. Then the thermal strain of each component at 460 K before soldering was calculated. The thermal strain for the REBCO layer is provided at step B2 in table 4. At the soldering temperature (T_s), the solder keeps liquid state and then solidifies during cooling. Solder shrinks during solidification and during cooling under the constraint condition as a component of the composite. In the present calculation, the solder was presumed to give minimum influence to the change of local strain on the SC component, because the solder layer was very thin and so soft mechanically.

(c) Steps B2–B3–B4: thermal strain on REBCO layer at 293 and 77 K for the tape mounted on SB.

The thermal strain on component i of the tape mounted on the SB after cooling to temperature T is given by;

$$A_i^T = A_i^{Ts} + \int_T^{Ts} (\alpha_i - \alpha_c)\mathrm{d}T, \qquad (10)$$

where $T_i^{Ts}$is given by equation (9). Given the tape cools down on the SB, the constraint condition equivalent to equation (6) holds where six components are included—the five components listed in table 5 as well as the Cu–Be of the SB which takes up 98.74% and 98.78% of the total volume for the Superpower and SuNAM configurations, respectively. The

thermal strain values at steps B3 and B4 for the two tapes are listed in table 4 from which it is possible to evaluate the local strain exerted on the REBCO layer at 77 K, when applying a uniaxial strain. As given by equation (3), the local strain on the REBCO layer at 77 K is the sum of the lattice strain and thermal strain. We assume the slope, dA^{lat}_{REBCO}/dA_a is the same at 77 K as that at room temperature, where average values from the different directions listed in table 3 were used. The calculated results for the SuperPower tape and the SuNAM tape are shown in figure 7. This relationship between the local strain (with reference to zero thermal strain state at 77 K) exerted on the REBCO layer as a function of applied strain at 77 K is used in the next section in the discussion of the local strain dependence of the critical current.

3.4. Critical current measurements and analysis

3.4.1. Measurements of the applied strain dependence of the critical current for the tapes. The *E–I* characteristic of high current superconductors is empirically described by the equation

$$E = E_c\left(\frac{I}{I_c}\right)^n, \tag{11}$$

where E_c is the electric field at which the critical current I_c is defined and n is known as the index of transition. Previous studies [10, 22] have shown that the I_c of REBCO tapes decreases gradually over a small range of tensile strains and that the critical current returns reversibly on reducing the strain. When the tensile strain increased beyond the reversible limit, the critical current decreased rapidly due to the brittle fracture of REBCO layer. In the present study, this behaviour was confirmed as shown in figure 8.

The critical current measurements were carried out using the following sequence. During cooling, careful control of the universal testing machine ensured that no external strain was applied to the tape sample. First the critical current was measured at zero applied strain (I_{c0}). In the second step, a strain was applied and I_c was measured. Then the applied strain was reduced to zero and what we denote the 'recovered critical current' (I_{cr}) was measured again as shown in figure 8. Further critical current measurements were repeated in this cyclic fashion by increasing the applied strain, step by step. The sequence of critical current measurements for the Superpower tape mounted on a SB is shown in figure 8(a). After measuring I_{c0}, compressive strain was applied and I_c was measured. Then the stress was released to zero and I_{cr} was measured. After reaching about −0.5% compressive strain, the applied strain was released to zero. Then tensile strains were applied from zero to +0.5% step by step. Figure 8(b) also shows results in the tensile strain region for the freestanding SuNAM tape. Similar measurements were made with the SuNAM tape on a SB as well as on a freestanding Superpower tape. The initial n-values and I_c values obtained from the *E–I* characteristics for these tapes are listed in table 6.

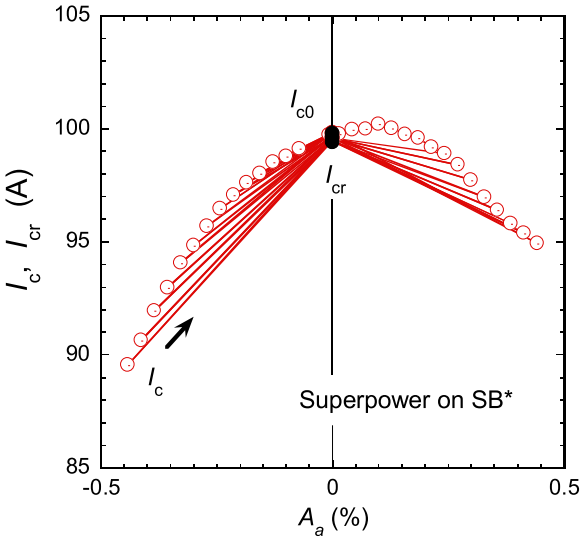

(a) Superpower tape mounted on a SB (I_{c0}=99.6A)

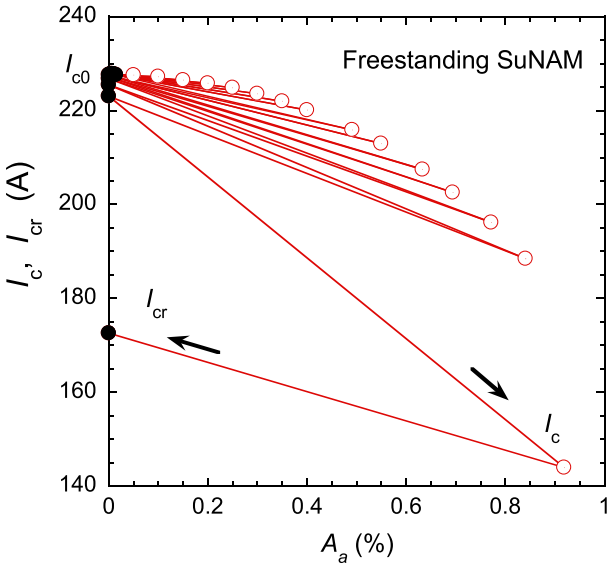

(b) Freestanding SuNAM tape (I_{c0}=227A)

Figure 8. Critical current as a function of applied strain. (a) Superpower tape mounted on a SB (I_{c0} = 99.6 A). (b) Freestanding SuNAM tape (I_{c0} = 227 A).

Table 6. Initial I_{c0} and n-values for the two tapes in both freestanding and SB configuration. Also shown are 95% I_c retained strain and 99% I_{cr} recovered strain.

	Superpower	SuNAM
I_{c0} (A)—Freestanding	94.5	227
n-value—Freestanding	23	42
I_{c0} (A)—SB	99.6	206
n-value—SB	25	34
$A_a(I_c/I_{c0} = 0.95)$ (%)—SB	0.41	0.48
$A_a(I_{cr}/I_{c0} = 0.99)$ (%)—SB	0.45	0.78
$A_a(I_{cpeak})$ (%)—SB	0.092	−0.063

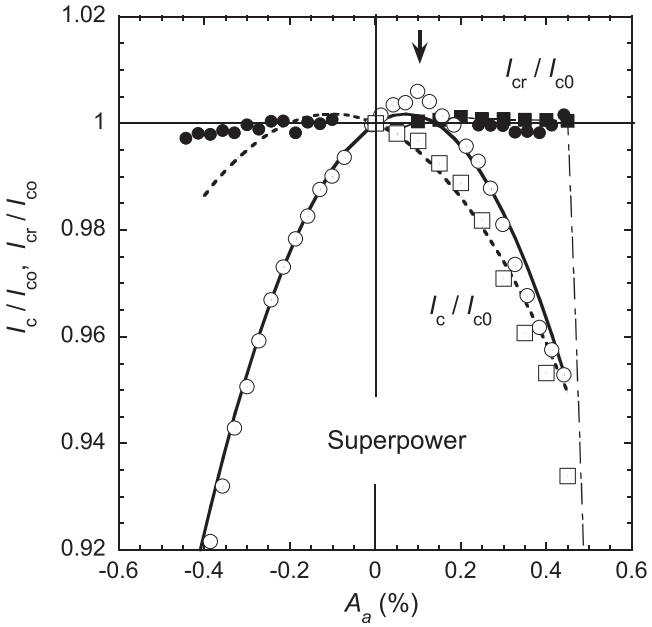

(a) Superpower

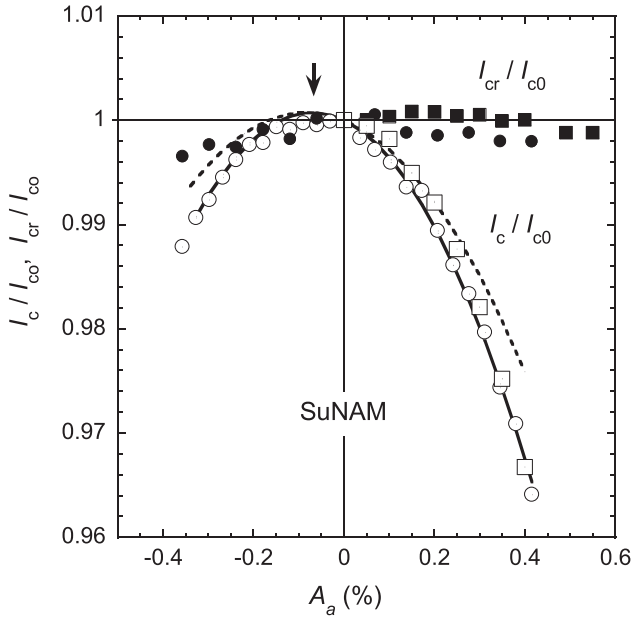

(b) SuNAM

Figure 9. A comparison of the normalized critical currents, I_c/I_{c0} and I_{cr}/I_{c0} versus applied strain at 77 K for the Superpower tape and the SuNAM tape in both the freestanding (■, □) and springboard(●, ○) configurations. The solid and dotted curves are the curve fitted results by using equation (12). (a) Superpower (b) SuNAM.

Normalized critical currents, I_c/I_{c0} and I_{cr}/I_{c0} are plotted as a function of applied strain in figure 9(a) for the Superpower tape. In the freestanding configuration, the normalized recovered critical current I_{cr}/I_{c0} as indicated by ■ kept almost constant at unity up to about 0.45% and then decreased abruptly. As linked by the dashed line, the next data points at $A_a = 0.5\%$ recorded $I_c/I_{c0} = 0.79$ and $I_{cr}/I_{c0} = 0.89$. The normalized critical current I_c/I_{c0} decreased gradually from the beginning and then decreased rapidly associated with the abrupt drop of I_{cr}/I_{co} and the brittle failure of the REBCO layer. Within the strain region investigated on the SB, namely −0.5% and 0.5%, the normalized recovered critical current I_{cr}/I_{c0} was almost unity, which means there was no degradation. Figure 9(b) also shows the equivalent normalized critical currents, I_c/I_{c0} and I_{cr}/I_{c0} as a function of applied strain for the SuNAM tapes both freestanding as well as on a SB. Beyond A_a ($I_{cr}/I_{c0} = 0.99$) = 0.78% even though no data is indicated here, both I_c/I_{c0} and I_{cr}/I_{c0} decreased rapidly for the freestanding SuNAM tape due to the brittle fracture of REBCO layer. The four sets of I_c/I_{c0} data in figures 9(a) and (b) have been accurately fitted using a second order polynomial as mentioned later (see equation (12)).

There are two criteria that can provide useful practical strain limits for using high temperature superconducting tapes. Given that the recovered critical current I_{cr} decreased rapidly beyond a certain strain as the REBCO fractured, the reversible strain limit can be characterized using the strain at which $I_{cr}/I_{c0} = 0.99$ [2]. As listed in table 6, $A(I_{cr}/I_{c0} = 0.99)$ was 0.45% and 0.78% for the Superpower and SuNAM tapes respectively. Alternatively one can cite the strain at which the current density drops to 95% of the original critical current ($A(I_c/I_{c0} = 0.95)$). In this case, the retained strain was 0.41% and 0.48% for the Superpower and SuNAM tapes respectively. In several publications [10, 23], the 95% retained strain ($A(I_c/I_{c0} = 0.95)$) limit has been reported as the reversible strain limit for both REBCO and BSCCO tapes. In the case of BSCCO tapes, it has been reported to use the 95% retained strain ($A(I_c/I_{c0} = 0.95)$) as the reversible strain limit [24, 25]. However as shown by the data in table 6, in the case of REBCO tapes, the strain limit is best defined using the 99% I_{cr} recovered strain ($A(I_{cr}/I_{c0} = 0.99)$) [26, 27] to exploit the full potential of the both tapes and avoid REBCO fracture.

For both tapes, the I_c data on the SB are not symmetric. For the Superpower tape the centre of the convex curve on the SB is located in the tensile strain region whereas since the freestanding I_c data monotonically decreases on applying strain, the peak for the freestanding sample can be expected to be in the compressive strain region and hence there is a shift in the position of the strain at which the peak in I_c occurs between these two measurements. In contrast, for the SuNAM tape, both measurements give the peak to be in the compressive side.

3.4.2. Local strain and consistency between different types of measurements. As has been long established and is outlined in Ekin's textbook [28], the strain dependence of the critical current in low temperature superconductors is a function of the thermodynamic critical parameters T_c and B_{c2}. The strain dependence of Nb_3Sn has been investigated in most detail because of its importance in high field applications. The usual explanation for the position of the maximum I_c in the strain dependency curve [7, 29–34], is related to the zero deviatoric strain associated with the anharmonic terms in the lattice vibration. For polycrystalline Nb_3Sn material, when there is no net force on the material, we find the values of T_c and B_{c2}

to be optimum values. Hence the highest superconducting properties are found in a freestanding composite wires when there is good thermal matching between the components of the composite and the superconductor. In measurements on such round wires mounted on a sample holder, the contact between the sample holder and the wire can be almost a one-dimensional line contact. After cool-down to the operating temperature, the peak in I_c occurs when the applied strain compensates for any thermal precompression or tension from the sample holder. We can consider this in terms of local strain: if the free standing wire does not have the same CTE as the sample holder, there is a one-dimensional thermal strain on the wire. To first order there is no thermal strain orthogonal to the direction of the line contact. Hence by applying uniaxial strain, one can almost completely compensate for the one-dimensional thermal strain and achieve zero local strain both parallel and orthogonal to the applied strain. This explanation is supported by the universal behaviour observed as a function of intrinsic strain for Nb_3Sn samples mounted on brass, steel, Cu–Be and Ti-alloy sample holders [34]. In the limit that the wire is attached along a perfectly thin line-contact to the sample holder, any differences in the Poisson ratio between the sample holder and the wire (see tapes below) play no role in measuring the uniaxial strain dependence of I_c in the wire. Recently, we reported neutron [9] and synchrotron [21] results on the local strain of Nb_3Sn filaments in an ITER strand and found that, the force-free strain (A_{ff}) along the wire axis was indeed (almost) consistent with the peak strain (A_p) at which I_c reaches its maximum value predictions [9, 21]. On the other hand, the peak strain (A_p) did not exactly coincide with the force-free strain along the transverse direction [9]. This result reminds us that to understand Nb_3Sn wires in finer detail, we must consider more quantitatively the inhomogeneous local three dimensional strain distribution in the composite wires.

Measurements on tapes mounted on sample holders are more complex than made those on round wires because of the two-dimensional contact area with the sample holder. For both the freestanding measurements and in the measurements on the SB in this work, it is not possible to compensate for the large thermal strain (see table 2) in directions both parallel and orthogonal to the applied uniaxial strain. In fact if one reduces the local compressive strain along the direction of the applied strain, the local compressive strain increases in the orthogonal direction and as we discuss below, in general this tends to drive I_c further away from its peak value.

The microstructure of the REBCO in the tapes we have investigated has been measured and found to consist of two distinct populations of twinned domains with the *a*-axis of any unit cell either parallel or orthogonal to the applied tensile strain [35]. Single crystal data on YBCO show that if the *a*-axis is parallel to the applied strains, T_c will increase with increased tensile strain whereas it will decrease for those domains with their *a*-axis orthogonal to applied tensile strains. Also strain in the *c*-direction has little effect on T_c—at least and order of magnitude smaller than in the *a*- or *b*-directions [36]. This behaviour is also consistent with reports on detwinned (Y, Gd)BCO coated conductors [37]. This means although there are large thermal strains on all the domains at 77 K as listed in table 4, because the REBCO contracts almost isotropically, any change in T_c associated with a large local thermal strain in the *a*-direction of any unit cell (in either domain) is compensated for by an equal and opposite change in T_c associated with the equally large thermal strain in the *b*-direction. Hence to first order there is no change in T_c with an isotropic contraction of the REBCO. We initially follow van der Laan and assume that the material with the lowest T_c determines I_c [38], so that on applying a uniaxial strain (either compressive or tensile), T_c in one or other of the two domain populations decreases. Hence the condition for maximum I_c for two dimensional REBCO tapes with equal amounts of A-domains and B-domains, equivalent to force free condition for measurements on a polycrystalline Nb_3Sn round wire, is that the local strain (in orthogonal directions) ensures T_c of the two populations of domains in REBCO is the same. In general, because REBCO is broadly insensitive to volumetric strain, the peak is far from the force free state (in either direction) nor is it the condition that the *a*-axis equals the *b*-axis. Given the cubic Hastelloy substrate in the tape and the cubic Cu–Be of the SB contract isotropically, we can expect isotropic thermal contraction of the REBCO and no change in T_c associated with the unit cells contraction on cool-down. We can also consider the conditions necessary for the uniaxial strain dependence of I_c itself, in the two measurements using the freestanding tape and the tape mounted on SB to agree. Even though Poisson's ratio for Hastelloy ($\nu = 0.307$) [17] and Cu–Be ($\nu = 0.30$) [20] are reasonably close, when considering the influence of constituent components on the local lattice strain on the REBCO layer, we need to take care about the change of their volume fraction before and after mounting on SB as shown in tables 3 and 5. Furthermore as shown in figure 9, the thermally induced local strains for the freestanding tape and the tape mounted on SB are clearly very different from each other with commensurate large differences in unit cell volume. In this context even in Nb_3Sn composites where the effect of volumetric strain is also considered small, we find in experiments that the strain at which I_c is at a peak value occurs can change by 0.05% and the magnitude of I_c at the peak can vary by 5% if the components are made plastic during the measurements [39].

3.5. The chain model for a material with two types of domains

Most variable strain data in the literature can be described using a second order polynomial I_c data of the form:

$$\frac{I_c}{I_c(\beta = 0)} = 1 + c_1\beta + c_2\beta^2, \tag{12}$$

where β is the strain and c_1 and c_2 are constants. This is demonstrated for the data in this paper in figure 9. As mentioned in the introduction, the prevalence of the peak in I_c versus strain data found in most round wires has led many papers to report the critical current versus strain data in terms of intrinsic strain (A_i) where $\beta = A_i = A_a - A_p$ and the parameter A_p is related to the thermal precompression or pretension on superconductor in the wire. We show below

that the two-dimensional nature of the tape is important and that for the tapes measured in this work, we can best take $A_p = 0$ and hence $\beta = A_a$. Hence in this section, we consider equation (12) that treats strain in very general terms without making any initial assumptions about the thermal strain.

Consider a chain model for the REBCO material that has one-dimensional current flow. Within the chain, there are A-domains and B-domains oriented along the uniaxial strain direction [34] with fractional lengths of the two domains given by f and $(1 - f)$, respectively. We use the standard conventions so that within the A-domains, the unit cell has its a-lattice parameter parallel to the uniaxial strain which means the Cu–O chains are orthogonal to the uniaxial strain and vice versa for the B-domains. Given single crystal data show T_c increases in the A-domains under tensile strain, we have:

$$T_{c,A} = T_c(0) + \left(\frac{dT_{c,A}}{d\beta}\right)\beta. \quad (13)$$

Expanding about the $\beta = 0$ point for the A-domain, we have:

$$J_{c,A} = J_c(T, \beta) + \left(\frac{\partial J_c}{\partial T_{c,A}}\right)_T \partial T_{c,A}. \quad (14)$$

Equations (13) and (14) give:

$$J_{c,A} = J_c(0) + \left(\frac{\partial J_c}{\partial T_{c,A}}\right)_T \left(\frac{dT_{c,A}}{d\beta}\right)\beta = J_c(0)(1 + g\beta), \quad (15)$$

where $J_c(0)$ is the current density at zero strain at the operating temperature in the A-domain and g is positive. Rewriting equations (13)–(15) for the B-domains, we simplify the algebra by taking $J_c(0)$ and $T_c(0)$ to be the same in both domains. Hence the condition for a crossover in T_c and J_c between the two domains occurs when $J_{c,A}(0) = J_{c,B}(0) = J_c(0)$ and $T_{c,A}(0) = T_{c,B}(0) = T_c(0)$ and when $\beta = 0$. From the single crystal data, we know that $dT_c/d\beta$ has opposite signs for the two domains and there is an equal and opposite change in J_c from $J_c(0)$ within the two populations when strain is applied. Using equation (11), we can calculate the value of J_c at the standard E-field criterion, given that the electric fields generated in each domain change and that the current is constant along the chain. When the average E-field along the chain is E_c, we have:

$$1 = f\left\{\frac{J_c}{J_c(0) + \Delta J_c}\right\}^n + (1 - f)\left\{\frac{J_c}{J_c(0) - \Delta J_c}\right\}^n, \quad (16)$$

where ΔJ_c is the change in the critical current density in the A-domain as a result of applying strain and given by $\Delta J_c = \left(\frac{\partial J_c}{\partial T_{c,A}}\right)_T \left(\frac{dT_{c,A}}{d\beta}\right)\beta = J_c(0)g\beta$. The parameter f gives the fraction of A-domains in the chain. The upper panel of figure 10 shows data generated using equation (16) for different values of the index of transition n where we have assumed equal fractions of A-domain and B-domain (i.e. $f = 0.5$). Inverted parabolic behaviour is observed, consistent with the experimental data. In the lower panel of figure 10, we have taken a typical value of the index of transition (i.e. $n = 25$) and using equation (16) have calculated J_c for different values of f. The figure shows how the position of the peak in J_c moves from zero strain, as the relative populations change. Writing equation (16) in terms of I_c for the chain

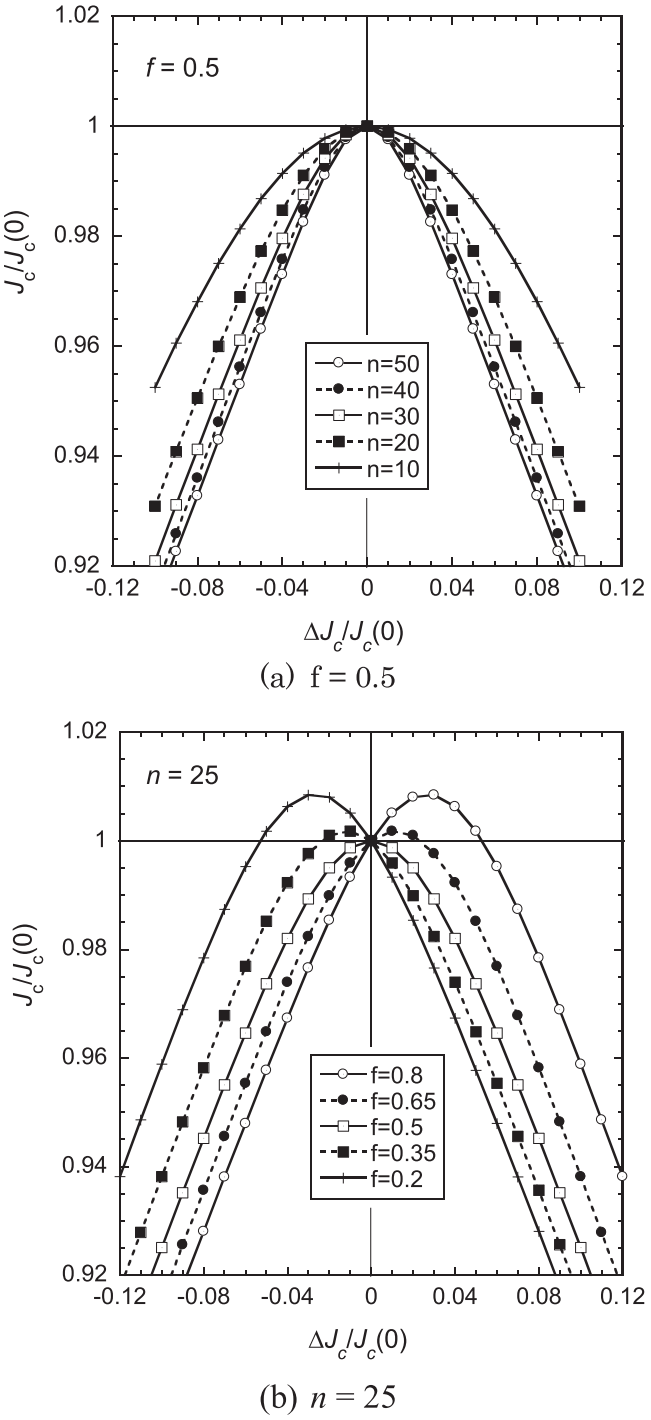

Figure 10. A calculation of the normalized critical current density for a material with two populations of A- and B-domains contributing to J_c. The x-axis is the fractional change in J_c in these populations. (a) $f = 0.5$ (b) $n = 25$.

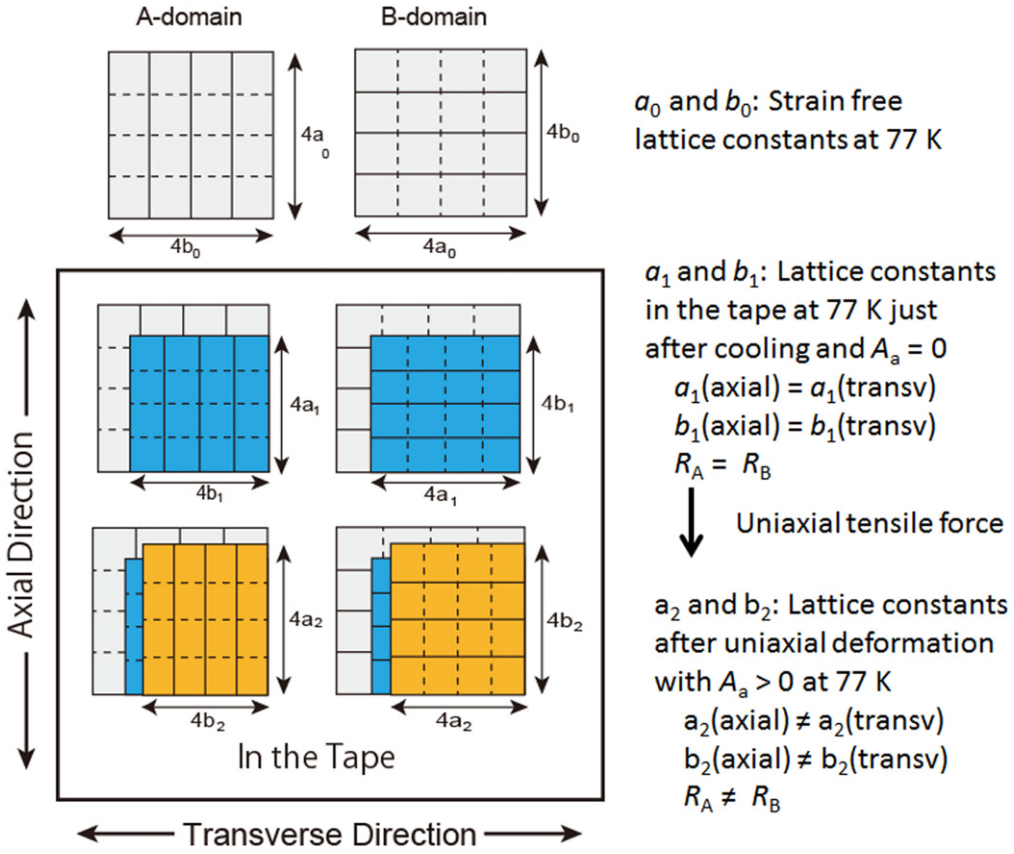

Figure 11. The change of lattice constants due to the cooling as well as the uniaxial deformation. Here the shape of a 4 × 4 REBCO set of unit cells in the A-domain and in the B-domain of a REBCO tape is given. The dotted lines in the domains denote the direction of the Cu–O chains.

material, for small strains we find

$$I_c = I_c(0)\{1 - (1-2f)g\beta - 2(1-f) f(1+n)g^2\beta^2 + O[\beta^3]\}. \quad (17)$$

Equations (12) and (17) can also be written in the form:

$$\frac{J_c}{J_c(0)} = 1 - \gamma(\beta - \beta_{peak})^2 + \gamma\beta_{peak}^2, \quad (18)$$

where γ and β_{peak} are constants. Comparing equations (12), (17) and (18) we have

$$\beta_{peak} = -\frac{c_1}{2c_2} = -\frac{(1-2f)}{4(1-f)f(1+n)g} \quad (19)$$

and

$$\gamma = -c_2 = 2(1-f)f(1+n)g^2 \quad (20)$$

which gives: β_{peak} is zero when either $f = 0.5$ or when the index n tends to infinity, and also β_{peak} is infinite if the material is perfectly textured (i.e. $f = 0$ or $f = 1$). Equation (19) shows that if the material has more A-domains, the peak appears on the tensile side (i.e. $\beta > 0$). If the material has more B-domains, the peak is on the compressive side.

3.6. Parameterization of the strain dependence and the peak of the critical current data

3.6.1. Coincidence in T_c in the two populations of domains. Section 3.5 has considered a one-dimensional chain model which includes a strain parameter β which, by definition, is zero when there is coincidence of T_c in the two different domains. Figure 11 gives an indication of what the shape of the REBCO unit cells is like in the A-domains and the B-domains under various conditions. In the thermal strain free state, the unit cells in both domains are not strictly cubic, but have an oblong shape because the lattice constant b is larger by about 1.4% than the a lattice constant. In order to identify the conditions for the coincidence of T_c in the two domains, we introduce the factor R which is defined as the ratio of the lengths of the unit cell in the a-direction and the b-direction. In A-domain:

$$R_A = \frac{\text{Length of unit cell in } a\text{−direction}}{\text{Length of unit cell in } b\text{−direction}} \quad (21)$$

and there is a similar expression for B-domain. When the tape is cooled down and the REBCO contracts isotropically, the a- and b-lattice constants broadly reduce by the same amount. The unit cells in both domains experience an isotropic (2D) contraction—the reduction in T_c caused by the contraction of the a-lattice parameters is compensated by the increase in T_c caused by the contraction of the b-lattice parameters. Hence

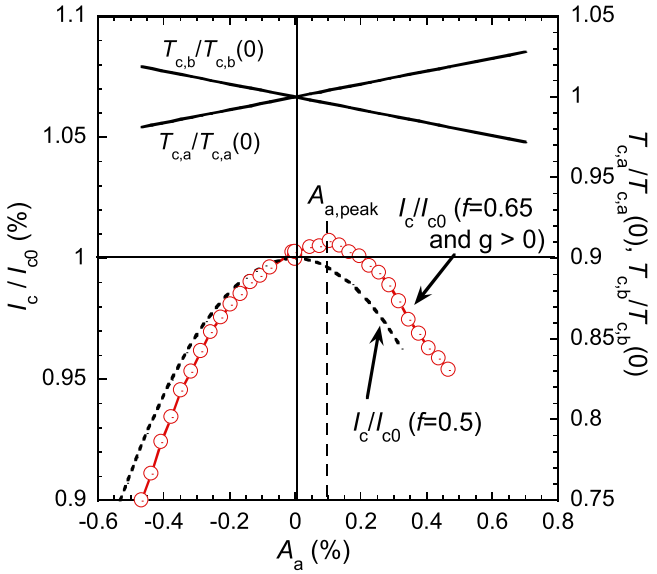

Figure 12. Schematic relation for the critical current and critical temperature as a function of the applied strain.

Table 7. Strain at the critical current maximum and parameterization of the tape mounted on a SB and the freestanding tape using equation (12) to find a and b and equation (17) to find f and g, using the index of transition values (n) for the two tapes. The value of $A_a(I_{cpeak})$ enclosed in brackets was obtained from equation (19). The thermal strain ($A_{REBCO}{}^T$) at 77 K is evaluated from figure 7.

	Superpower		SuNAM	
	On SB	Free standing	On SB	Free standing
$A_a(I_{cpeak})$ (%)	0.073	(−0.11)	−0.074	(−0.067)
n	25	23	34	42
c_1	0.0500	−0.0348	−0.0210	−0.0176
c_2	−0.353	−0.158	−0.150	−0.131
f	0.645	0.355	0.390	0.390
g	0.172	0.12	0.095	0.080
$A_{REBCO}{}^T$ (%)	−0.42	−0.18	−0.38	−0.12

$R_A \approx R_B$ and we can expect $T_{c,A} \approx T_{c,B}$. As shown at the bottom of figure 11, when applying a uniaxial strain along the tape axis, both A and B domains elongate in the axial direction and shrink in the transverse direction due to Poisson's law. Such anisotropic deformation results in $R_A \neq R_B$ which gives the condition of $T_{c,A} \neq T_{c,B}$. Hence we conclude that under the approximations considered, for the REBCO tapes, the coincidence in T_c in the two domains occurs at $A_a = 0$ (i.e. $\beta = A_a$). Beyond these approximations of isotropic contraction and compensation of changes in T_c, one can expect anisotropy in the superconducting and physical properties of the HTS, and thermal and mechanical mismatch between the non-superconducting materials that are integral to the measurement. Hence the coincidence of T_c in the two domains can then occur at non-zero applied strain.

3.6.2. Parameterization of the variable-strain I_c data. Figure 9 demonstrates that the parabolic equation (equation (12)) fits the experimental data well. The parameters derived from these fits are listed in table 7 as well as the parameters derived from equations (17) and (18) using the n-values given in table 6. We can develop our discussion about how to relate the parameters derived in the I_c measurements to the synchrotron radiation data, using equation (17) and the schematic illustration shown in figure 12 where the experimental data for the Superpower tape mounted on the SB are re-plotted as a function of the applied strain. The maximum strain $A_{a,peak}$ is located in the tensile applied strain region. As indicated by equation (13), in this analysis $T_{c,A}$ and $T_{c,B}$ cross each other at $A_a = 0$. The value of the peak depends on the fraction f and the parameter g as indicated equation (19). When f is 0.5, the maximum strain is located at $A_a = 0$. When f increases beyond 0.5, $A_{a,peak}$ shifts towards the tensile applied strain and the maximum value of I_c increases. Equally, the peak in I_c occurs on the compressive side for the SuNAM tape on the SB, where f is smaller than 0.5.

We have also found fitted values of f and g using equation (16) directly. Best fits to the data are found by restricting the fits to the strain near the peak and similar values were found to those in table 7. At high strains, equation (16) describes a linear strain behaviour for I_c associated with dissipation predominantly in a single domain and the linear approximations made, for example in equation (15). As shown in figure 9, the I_c data can be accurately described using a second order polynomial out to high strains, consistent with the eventual break-down of the linear approximations. Hence below, we consider the values of f and g given in table 7 derived from the polynomial fits. We also considered the effects of introducing an additional free parameter that allows the possibility of a non-isotropic thermal strain (i.e. $\beta = A_a - h$ where h is the uniaxial thermal strain necessary to produce coincidence in T_c in the two domains). However the values for f, g and h were very strongly correlated, giving a very wide range of parameters with almost equally good fits to the data. These correlations confirmed the importance of combining I_c measurements with synchrotron measurements to determine independently the nature of the thermal pre-strain (i.e. h).

3.6.3. f-values. As mentioned above, one has to be careful about a qualitative analysis of the diffraction data. Nevertheless, the peak in I_c that occurs on the compressive side for the SuNAM tape in both freestanding and SB configurations and for the freestanding Superpower tape, is consistent with more B-domains than A-domains and the larger (020) peaks in figure 4. However, although the relative height of the (020) peak is somewhat reduced in the freestanding Superpower data compared to the Superpower SB data, it is not larger than the (200) peak which is required to explain the peak in I_c observed on the tensile side for the Superpower tape. As listed in table 6, the critical currents (I_{c0}) measured initially at the zero applied strain were different for

the free standing tape and the tape mounted on SB. Their difference is 5% and 10% for Superpower and SuNAM tapes, respectively. The change is an increase in I_c for the Superpower tape but a decrease in I_c for the SuNAM tape. These results open the questions of what the origins of these differences are and how best to normalize I_c if they occur. The differences can be attributed to: scatter in the I_c data related to measurement errors; inhomogeneity of properties along the length of the tapes; changes caused during the mounting and soldering procedure and the approximations made about the isotropy of the component materials in the tape and SB in these measurements. We are investigating better mounting procedures using low temperature solders with good mechanical properties as part of achieving the requirement for I_c measurements with an accuracy and reproducibility of better than 1% [40].

3.6.4. g-values. Assuming a reasonable and simple temperature dependence for I_c of the form $I_c = I_c(0)(1 - T/T_c)^{1.5}$ (where $I_c(0)$ is a constant given that $T_c = 92$ K and that I_c increases typically by a factor of ~20 on reducing the temperature from 77 to 4.2 K), equation (15) gives

$$g = \left(\frac{1}{J_c(0)}\right)\left(\frac{\partial J_c}{\partial T_c}\right)_T\left(\frac{dT_c}{dA_a}\right) = \frac{3T}{2T_c^2(1 - T/T_c)}\left(\frac{dT_c}{dA_a}\right). \quad (22)$$

Using $T = 76.9$ K, $T_c = 92$ K and $\frac{dT_c}{dA_a} = 2.2$, equation (22) gives $g = 0.18$ which is in satisfactory agreement with the values for g in table 7. We can expect some differences between g derived from single crystal data and those measured for the tapes because of the large content of inclusions in the tapes that increase I_c. When cooling down to 77 K and at the zero applied strain, the thermal strain exerted on REBCO layer is shown in figure 7 and their value is listed in table 7. The thermal strains for the tapes mounted on SB were larger than those for the freestanding tapes. The REBCO layer for the tape on SB sustains much larger isotropic compressive strain than that for the freestanding tape. We note that a hydrostatic pressure will play a role and that the g value increases systematically with increasing the compressive thermal strain exerted on REBCO layer as shown in table 7.

4. Discussion

4.1. The mechanism that determines the critical current

From a macroscopic viewpoint, a practical REBCO tape is composed of well controlled single-crystalline-like two dimensional structures with thickness of a few μm connected via low-angle grain boundaries. It may also have weak links which originate from high angle grain boundaries and are minimized in number as much as possible during fabrication. On the microscopic scale however, twin boundaries occur throughout the grains as well as non-SC pinning centres. In the tapes investigated in this work, their Ginzburg–Landau constant and their current densities are so high that even in zero applied field, most of the material is in sufficiently high self-field that the SC is in the mixed state, well-above its lower critical field. Such considerations remind us that we do not yet have an accurate description of the dissipative state of I_c in zero applied field and to what degree fluxon anti-fluxon annihilation or fluxons transversing the entire sample are important.

Furthermore the mechanism that determines the critical current is not agreed either. In the standard pinning model, one usually considers non-superconducting or weakly superconducting precipitates that hold or pin single quantized magnetic flux lines [41]. Pinning models can also incorporate so-called collective pinning or flux shearing where the elastic constants of the flux line lattice are also included [42]. We are investigating the flow of fluxons along channels in which the simultaneous movement of several fluxons is important as well as the topology of the flux flow. Determining the details of the mechanism that determines the critical current and the nature of the dissipative state are important because they guide our approach to increasing the operating current of a superconductor in applications. Unfortunately, at this moment, there are sufficient free parameters in both standard flux pinning models and the models that consider flux flow along channels that both can equally well describe most of the limited data that the community has produced. We are putting significant effort into developing the mathematical framework for flux flow along channels. As the community develops better experimental tools to measure the local structural and chemical homogeneity along channels between pinning sites, and completes more comprehensive I_c measurements on many different samples, we expect that it will become increasingly apparent that the local properties of the channels, along which flux flows, will need to be explicitly included in any accurate description of current density [43, 44].

4.2. The functional form of the critical current under strain

Historically, measurements on Nb_3Sn have been used to develop the framework for the strain dependence of J_c in high field superconductors. For some decades, the class of A15 materials held the record value for the highest T_c known. This was attributed to the fortunate coincidence of the Fermi energy in these materials occurring at the peak in the electronic density of states. It was reasonable at that time to assume the peak in J_c under force free conditions was also the coincidental occurrence of the peak in the density of states. However the measurements on single crystals of Nb_3Sn show anisotropic behaviour [45] reminiscent of the data for single crystals of REBCO [36]. Naturally this opens the possibility that the peak in J_c found in both Nb_3Sn (LTS) and REBCO (HTS) polycrystalline materials has the same origin—broadly explained by the peak occurring when there is uniform T_c throughout the material (or at least a minimum in the width of the distribution of T_c) and an inverted quasi-parabolic

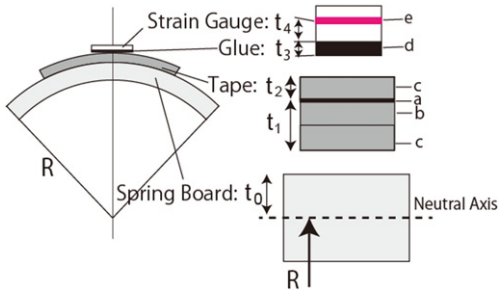

Figure A1. The detail of the strain applied by using the springboard, where (a)–(e) are the superconducting layer, substrate, lamination layer, glue and sensing element of the strain gauge.

behaviour associated with anisotropic properties and broadly described in section 3.5.

5. Conclusion

By measuring two kinds of practical REBCO tapes using two different I_c measurement techniques, we have found the uniaxial strain dependence of the critical current. One of the techniques had the sample attached directly to the universal testing machine and is pulled by tensile load. The other used a SB on which the sample is soldered, is attached the testing machine and then is pushed or pulled in order to apply both tensile and compressive strains to the tape sample. In particular, a parabolic behaviour was observed in the uniaxial strain dependence for both tapes. The normalized critical current was plotted as a function of the applied strain.

Using synchrotron radiation, the local strain exerted on the REBCO layer was measured at room temperature using the same two techniques for straining the tape as for I_c measurements. On the basis of their observed data at room temperature, the local strain exerted on the REBCO layer at 77 K was numerically evaluated.

A one-dimensional chain model for REBCO material with fractional lengths of A-domains and B-domains oriented along the uniaxial strain direction has been proposed. The approach shown can reproduce the broad features of the experimental results on the uniaxial strain dependence of the critical current.

Acknowledgments

This work was supported in part by a grant-in-aid of the Ministry of Education, Culture, Sports, Science and Technology, Japan (26420669) and EPSRC grant EP/K504178/1 for the Fusion Doctoral Training Network. The authors express their hearty thanks to VAMAS-TWA16 for supplying the samples. The synchrotron radiation experiments were performed at the BL45XU of SPring-8 with the approval of the Japan Synchrotron Radiation Research Institute (JASRI) (Proposal No. 2014A1553). We acknowledge discussions with Paul Branch. The data are available at: http://dx.doi.org/10.15128/gh93gz499.

Table A1. Parameters for evaluating the factor k.

	Superpower	SuNAM
t_0 (mm)	1.25	1.25
t_1 (mm)	0.075	0.13
t_2 (mm)	0.020	0.060
t_3 (mm)	0.015	0.015
t_4 (mm)	0.040	0.040
k	0.946	0.923

Appendix. Correction of the strain measured by means of the SB

The strain gauge was attached on the tape surface as shown in figure A1. The applied strain measured by means of the strain gauge is given as

$$A_{SG} = \frac{t_0 + t_1 + t_2 + t_3 + t_4}{R} 100 \quad [\%], \tag{A1}$$

where t_0 is the half-thickness of the SB, t_1 is the distance from the bottom surface to the superconducting layer, t_2 is the thickness of the Cu lamination, t_3 is the thickness of the glue and t_4 is the half-thickness of the strain gauge.The applied strain on the superconducting layer is given as

$$A_{SC} = \frac{t_0 + t_1}{R} 100 \quad [\%]. \tag{A2}$$

In order to evaluate the applied strain (A_{SC}) on the superconducting layer from the strain (A_{SG}) measured by means of the strain gauge, a correction is necessary as follows

$$A_{SC} = kA_{SG} \tag{A3}$$

And the factor k is given as

$$k = \frac{t_0 + t_1}{t_0 + t_1 + t_2 + t_3 + t_4}. \tag{A4}$$

The values of those parameters for Superpower and SuNAM are given in table A1.

References

[1] International Electrotechnical Commission 2014 Superconductivity- Superconducting wires—Categories of practical superconducting wires—General characteristics and guidance *Technical report* IEC TR 61788-20:2014 Ed. 1.0

[2] Osamura K, Machiya S, Tsuchiya Y and Suzuki H 2010 Force free strain exerted on a YBCO layer at 77 K in surround Cu stabilized YBCO coated conductors *Supercond. Sci. Technol.* **23** 045020–6

[3] Osamura K, Machiya S, Suzuki H, Ochiai S, Adachi H, Ayai N, Hayashi K and Sato K 2008 Mechanical behavior and strain dependence of the critical current of DI-BSCCO tapes *Supercond. Sci. Technol.* **21** 054010–8

[4] Osamura K, Machiya S, Tsuchiya Y, Suzuki H, Shobu T, Sato M and Ochiai S 2012 Microtwin structure and its influence on the mechanical properties of REBCO coated conductors *IEEE Trans. Appl. Supercond.* **22** 8400809

[5] Osamura K *et al* 2013 Thermal strain exerted on superconductive filaments in practical Nb_3Sn and Nb_3Al strands *Supercond. Sci. Technol.* **26** 094001

[6] Oguro H, Awaji S, Watanabe K, Sugano M, Machiya S, Shobu T, Sato M, Koganezawa T and Osamura K 2012 Internal strain measurement for Nb_3Sn wires using synchrotron radiation *Supercond. Sci. Technol.* **25** 054004

[7] Ekin J W 1980 Strain scaling law for the flux pinning in practical superconductors: 1. Basic relationship and application to Nb_3Sn conductor *Cryogenics* **20** 611

[8] Cheggour N, Nijhuis A, Krooshoop H J G, Lu X F, Splett J, Stauffer T C, Goodrich L F, Jewell M C, Devred A and Nabara Y 2012 Strain and magnetic-field characterization of a bronze-route Nb_3Sn ITER wire: benchmarking of strain measurement facilities at NIST and university of twente *IEEE Trans. Appl. Supercond.* **22** 4805104

[9] Osamura K, Machiya S, Harjo S, Nakamoto T, Cheggour N and Nijhuis A 2015 Local strain exerted on Nb_3Sn filaments in an ITER strand *Supercond. Sci. Technol.* **28** 045016

[10] Osamura K, Machiya S, Tsuchiya Y and Suzuki H 2010 Internal strain and mechanical properties at low temperatures of surround Cu stabilized YBCO coated conductor *IEEE Trans. Appl. Supercond.* **20** 1532–6

[11] Osamura K, Machiya S, Hampshire D P, Tsuchiya Y, Shobu T, Kajiwara K, Osabe G, Yamazaki K, Yamada Y and Fujikami J 2014 Uniaxial strain dependence of the critical current of DI-BSCCO tapes *Supercond. Sci. Technol.* **27** 085005

[12] Sunwong P, Higgins J S and Hampshire D P 2011 Angular, temperature and strain dependencies of the critical current of DI-BSCCO tapes in high magnetic fields *IEEE Trans. Appl. Supercond.* **21** 2840–4

[13] http://superpower-inc.com/content/2g-hts-wire

[14] http://i-sunam.com/home/en_company,4,1,4,4

[15] Osamura K, Sugano M, Machiya S, Adachi H, Ochiai S and Sato M 2009 Internal residual strain and critical current maximum of surrounded Cu stabilized YBCO coated conductor *Supercond. Sci. Technol.* **22** 065001–6

[16] Iijima Y, Onabe K, Futaki N, Tanabe N, Sadakata N, Kohno O and Ikeno Y 1993 Structural and transport properties of biaxially aligned $YBa_2Cu_3O_{7-x}$ films on polycrystalline Ni-based alloy with ion-beam-modified buffer layers *J. Appl. Phys.* **74** 1905

[17] Database of Hastelloy appeared in (www.haynesintl.com/HASTELLOYC276Alloy/HASTELLOYC276AlloyPP.htm)

[18] Ekin J W 2006 *Experimental Techniques for Low-Temperature Measurements* (Oxford: Oxford University Press)

[19] Database of AZO Materials in (www.AZO.com/properties.aspx)

[20] Japan Copper and Brass Association 1997 *Data Book of Cu and Cu-Alloy* (Tokyo: Japan Copper and Brass Association)

[21] Osamura K, Machiya S, Tsuchiya Y, Suzuki H, Shobu T, Sato M, Hemmi T, Nunoya Y and Ochiai S 2012 Local strain and its influence on mechanical- electromagnetic properties of twisted and untwisted ITER Nb_3Sn strand *Supercond. Sci. Technol.* **25** 054010

[22] Sugano M, Shikimachi K, Hirano N and Nagaya S 2010 The reversible strain effect on critical current over a wide range of temperatures and magnetic fields for YBCO coated conductors *Supercond. Sci. Technol.* **23** 085013

[23] Osamura K, Sugano M and Matsumoto K 2003 Mechanical property and its influence on the critical current of Ag/Bi2223 tapes *Supercond. Sci. Technol.* **16** 971–5

[24] Osamura K, Sugano M, Machiya S, Adachi H, Sato M, Ochiai S and Otto A 2007 Reversibility of micro-yielding and critical current in a YBCO-coated conductor caused by a uniaxial tensile load *Supercond. Sci. Technol.* **20** S211–6

[25] Osamura K, Machiya S, Suzuki H, Ochiai S, Adachi H, Ayai N, Hayashi K and Sato K 2009 Improvement of reversible strain limit for critical current of DI-BSCCO due to lamination technique *IEEE Trans. Appl. Supercond.* **19** 3026–9

[26] Osamura K *et al* 2009 Reversible strain limit of critical currents and universality of intrinsic strain effect for REBCO-coated conductors *Supercond. Sci. Technol.* **22** 025015–21

[27] Sugano M, Machiya S, Osamura K, Adachi H, Sato M, Semerad R and Prusseit W W 2009 The direct evalution of the internal strain of biaxially textured YBCO film in a coated conductor using synchrotron radiation *Supercond. Sci. Technol.* **22** 015002–8

[28] Ekin J W 2006 *Experimental Techniques for Low-Temperature Measurements* (Oxford: Oxford University Press)pp 432–55

[29] Muzzi L *et al* 2012 Direct observation of Nb_3Sn lattice deformation by high-energy x-ray diffraction in internal-tin wires subject to mechanical loads at 4.2 K *Supercond. Sci. Technol.* **25** 054006

[30] ten Haken B, Godeke A and ten Kate H H J 1999 The strain dependence of the critical properties of Nb_3Sn conductors *J. Appl. Phys.* **85** 3247

[31] Lu X F, Taylor D M J and Hampshire D P 2008 Critical current scaling laws for advanced Nb_3Sn superconducting strands for fusion applications with six free parameter *Supercond. Sci. Technol.* **21** 105016

[32] Arbelaez D, Godeke A and Prestemon S O 2009 An improved model for the strain dependence of the superconducting properties of Nb_3Sn *Supercond. Sci. Technol.* **22** 025005

[33] Taylor D M J and Hampshire D P 2005 The scaling law for the strain dependence of the critical current density in Nb_3Sn superconducting wires *Supercond. Sci. Technol.* **18** S241–52

[34] Taylor D M J and Hampshire D P 2015 Properties of helical springs used to measure the axial strain dependence of the critical current density in superconducting wire *Supercond. Sci. Technol.* **18** 356–68

[35] Osamura K, Machiya S, Tsuchiya Y, Harjo S, Suzuki H, Shobu T, Kiriyama K and Sugano M 2011 Internal strain behavior exerted on YBCO layer in the YBCO coated conductor *IEEE Trans. Appl. Supercond.* **21** 3090–3

[36] Uelp U, Grimsditch M, Fleshler S, Nessler W W, Downey J, Crabtree G W and Guipel J 1992 Effect of uniaxial stress on the superconducting transition in YBa_2CuO_7 *Phys. Rev. Lett.* **69** 2130

[37] Suzuki T, Awaji S, Oguro H and Watanabe K 2015 Applied strain effect on superconducting properties for detwinned (Y, Gd)BCO coated conductor *IEEE Trans. Appl. Supercond.* **25** 8400704

[38] van der Laan D C 2010 The effect of strain on grain boundaries in $YBa_2Cu_3O_7$ coated conductors *Supercond. Sci. Technol.* **23** 014004

[39] Taylor D M J and Hampshire D P 2004 Effect of axial strain cycling on the critical current density and n-value of ITER niobium–tin wires *Physica* C **401** 40–6

[40] Tsui Y, Surrey E and Hampshire D 2016 Soldered joints—an essential component of demountable high temperature superconducting fusion magnets *Supercond. Sci. Technol.* at press

[41] Collings E W 1986 *Applied Superconductivity, Metallurgy and Physics of Titanium Alloys* (New York: Plenum)
[42] Larkin A I and Ovchinikov Y N 1979 Pinning in type II superconductors *J. Low Temp. Phys.* **34** 409–28
[43] Carty G J and Hampshire D P 2013 The critical current density of an SNS junction in high magnetic fields *Supercond. Sci. Technol.* **26** 065007
[44] Sunwong P, Higgins J S, Tsui Y, Raine M J and Hampshire D P 2013 The critical current density of grain boundary channels in polycrystalline HTS and LTS superconductors in magnetic fields *Supercond. Sci. Technol.* **26** 095006
[45] McEvoy J P 1971 Effect of uniaxial stress on the superconducting transition temperature of monocrystalline Nb_3Sn *Physica* **55** 540–4